PCCP

PAPER

View Article Online
View Journal | View Issue

Cite this: *Phys. Chem. Chem. Phys.*, 2016, **18**, 24387

The influence of LiH on the rehydrogenation behavior of halide free rare earth (RE) borohydrides (RE = Pr, Er)†

Michael Heere,[a] Seyed Hosein Payandeh GharibDoust,[b] Christoph Frommen,[a] Terry D. Humphries,[ac] Morten B. Ley,[bd] Magnus H. Sørby,[a] Torben R. Jensen[b] and Bjørn C. Hauback*[a]

Received 28th June 2016,
Accepted 12th August 2016

DOI: 10.1039/c6cp04523e

www.rsc.org/pccp

Rare earth (RE) metal borohydrides are receiving immense consideration as possible hydrogen storage materials and solid-state Li-ion conductors. In this study, halide free $Er(BH_4)_3$ and $Pr(BH_4)_3$ have been successfully synthesized for the first time by the combination of mechanochemical milling and/or wet chemistry. Rietveld refinement of $Er(BH_4)_3$ confirmed the formation of two different $Er(BH_4)_3$ polymorphs: α-$Er(BH_4)_3$ with space group $Pa\bar{3}$, a = 10.76796(5) Å, and β-$Er(BH_4)_3$ in $Pm\bar{3}m$ with a = 5.4664(1) Å. A variety of $Pr(BH_4)_3$ phases were found after extraction with diethyl ether: α-$Pr(BH_4)_3$ in $Pa\bar{3}$ with a = 11.2465(1) Å, β-$Pr(BH_4)_3$ in $Pm\bar{3}m$ with a = 5.716(2) Å and $LiPr(BH_4)_3Cl$ in $I\bar{4}3m$, a = 11.5468(3) Å. Almost phase pure α-$Pr(BH_4)_3$ in $Pa\bar{3}$ with a = 11.2473(2) Å was also synthesized. The thermal decomposition of $Er(BH_4)_3$ and $Pr(BH_4)_3$ proceeded without the formation of crystalline products. Rehydrogenation, as such, was not successful. However, addition of LiH promoted the rehydrogenation of RE hydride phases and $LiBH_4$ from the decomposed $RE(BH_4)_3$ samples.

Introduction

In recent years, rare earth (RE) metal borohydrides have received increasing interest on a variety of research frontiers. Firstly, the hydrogen capacities of these materials, which vary between 9.0 wt% H_2 for $Y(BH_4)_3$ to 5.5 wt% H_2 for $Yb(BH_4)_3$, are highly comparable to the more established hydrogen storage materials, such as MgH_2 (7.6 wt% H_2) or $NaAlH_4$ (5.4 wt% H_2).[1–15] Secondly, RE borohydrides are also being pursued for other technological applications. For instance, their electrochemical properties have been investigated for solid state electrolytes in new battery applications,[16–19] novel optical and magnetic properties have also been identified.[20–22]

The established procedure for synthesizing RE borohydrides is the 'solvent-free' approach, where a RE-chloride and an alkali metal borohydride (Li, Na, K) are reacted in a one-step mechanochemical synthesis. $LiBH_4$ has, so far, proven to be the most efficient precursor during these reactions,[1–12,16,17,23] while attempts with other metal borohydrides, *e.g.* $NaBH_4$, generally offer poor yields at the most. This is perfectly illustrated in the recently reported synthesis of $Er(BH_4)_3$.[24] Meanwhile, the solvent based synthesis of metal borohydrides has been employed for over 50 years.[25] The advantage of this method is the ability to remove the byproducts (*e.g.* LiCl) to yield almost pure RE borohydride products, and thus allowing for the accurate determination of their physical properties.[1,14,16,26] The detriment of the solvent based synthesis is the possible decomposition of the RE borohydride upon removal of the solvent.[27] On the contrary, mechanochemical synthesis does allow for the facile synthesis of these materials without complicated *in vacuo* manipulations and possible decomposition of the desired product.[25]

A number of RE borohydrides (RE = La, Ce, Pr, Nd, Sm, Eu, Gd, Tb, Er, Yb, Lu) have been extensively characterized by *in situ* synchrotron radiation powder X-ray diffraction (SR-PXD), thermal analysis and vibrational spectroscopy.[2,13,14,24] In general, the materials can be categorized into several groups. RE = La, Ce and Nd form $LiRE(BH_4)_3Cl$ complexes crystallizing in space group $I\bar{4}3m$. In a recent study, Olsen *et al.*[13] demonstrated that mechanochemical manipulation of $PrCl_3$ and $LiBH_4$ only yields the $LiPr(BH_4)_3Cl$ complex. RE = Sm, Gd, Tb, Er and Yb form the corresponding $RE(BH_4)_3$, crystallizing in the space group $Pa\bar{3}$, which at high temperatures undergo a phase transition to form polymorphs in the space group $Fm\bar{3}c$. RE = Yb and Lu form $[RE(BH_4)_4]^-$ complex anions, which are stabilized by Li^+ cations

[a] *Physics Department, Institute for Energy Technology, NO-2027 Kjeller, Norway. E-mail: Bjorn.Hauback@ife.no*
[b] *Interdisciplinary Nanoscience Center (iNANO) and Department of Chemistry, University of Århus, Langelandsgade 140, DK-8000 Århus C, Denmark*
[c] *Department of Physics and Astronomy, Fuels and Energy Technology Institute, Curtin University, GPO Box U1987, Perth, 6845 WA, Australia*
[d] *Max-Planck-Institut für Kohlenforschung, Kaiser-Wilhelm Platz 1, DE-45470 Mülheim/Ruhr, Germany*

† Electronic supplementary information (ESI) available. See DOI: 10.1039/c6cp04523e

and are determined to crystallize in the space group $P\bar{4}2c$. Incidentally, the structures of the $[RE(BH_4)_4]^-$ complex anions are analogous to $ASc(BH_4)_4$ (A = Li, Na, K).[15,28–30] Furthermore, RE borohydrides (RE = Sm, Gd) react with LiCl to form $LiRE(BH_4)_3Cl$ complexes upon heating,[13] while trivalent RE = Sm and Eu in $LiRE(BH_4)_3Cl$ are reduced upon heating to divalent Sm and Eu ($RE(BH_4)_2$ (space group *Pbcn*)).[14]

The majority of the previous studies have been conducted on product mixtures containing both metal borohydrides and alkali metal chlorides, in most cases LiCl, making it virtually impossible to determine the specific effect of the halide salt on the pure metal borohydride. This is particularly related to reversible hydrogen sorption. For example, $Er(BH_4)_3$ was first synthesized from $ErCl_3$ and $LiBH_4$ by mechanochemical synthesis.[24] Thermal decomposition of the $Er(BH_4)_3$/LiCl product exhibited a hydrogen desorption of 3.4 wt%.[24] Rehydrogenation was achieved during absorption experiments applying $p(H_2)$ = 60 bar and T = 400 °C. Although the hydrogenation products were not determined in detail, it was stated that "$Er(BH_4)_3$ shows partial reversibility and reabsorbs about 20% of its original hydrogen content".[24] The present study illustrates that it is, surprisingly, the influence of LiH rather than LiCl or Li-ion which is responsible for reversible hydrogenation under the employed conditions.

In this study, $Er(BH_4)_3$ and $Pr(BH_4)_3$ have been synthesized halide free for the first time by mechanochemical and/or solvent techniques. The decomposition of both materials has been studied by *in situ* SR-PXD and the products and intermediates identified and their crystal structures determined by the Rietveld method. Moreover, thermogravimetric analysis (TGA) and differential scanning calorimetry (DSC), as well as mass spectrometry (MS) have been conducted. Finally, we have investigated the rehydrogenation behavior of $RE(BH_4)_3$ and decomposed $RE(BH_4)_3$ with addition of LiCl and/or LiH.

Experimental

Sample preparation

$LiBH_4$ (95%), $ErCl_3$ (99.9%), $PrCl_3$ (99.99%), dimethyl sulfide ($S(CH_3)_2$, anhydrous, 99.9%), diethyl ether ($(C_2H_5)_2O$, anhydrous, 99.7%) and toluene ($C_6H_5CH_3$, anhydrous, 99.8%) were purchased from Sigma Aldrich and used as received. Generally, a stoichiometric ratio of 1 : 3 $RECl_3$: $LiBH_4$ were reacted. The individual sample descriptions of the RE borohydrides analyzed in this study are presented in Table 1, including their reaction products, composition and lattice parameters determined by Rietveld refinements.

Mechanochemical synthesis (ball milling, BM) was executed using a Fritsch Pulverisette 6 planetary mill, employing an 80 ml tungsten carbide coated steel vial and balls with a ball to powder mass ratio of 40 : 1. Initially for samples S1 and S2, the powders were milled for 5 min followed by a break of 2 min at 400 rpm. After 24 repetitions, the reaction progress was determined by powder X-ray diffraction (PXD) followed by another 24 repetitions. The products were then dissolved in 20 ml $S(CH_3)_2$ per 1 g sample and stirred for three days. The LiCl was filtered from the solution and the $Er(BH_4)_3$ precipitated *in vacuo* using a rotary evaporator at 55 °C. To remove the coordinated $S(CH_3)_2$, the powder was heat treated at 145 °C in an oil bath, ground and heat treated once more. S2 was left under dynamic vacuum at 150 °C for 24 h. S1 was a light pink colored powder, whereas S2 was light orange.

S3 was synthesized by dissolving three molar equivalents of $LiBH_4$ per $PrCl_3$ in $(C_2H_5)_2O$ (60 ml per 1 g sample). After one day of stirring, the solution was filtered and the $(C_2H_5)_2O$ removed *in vacuo* using a rotary evaporator at 70 °C, yielding in a light green powder.

For S4, $PrCl_3$ was activated by ball milling using 20 repetitions of 5 min milling and 2 min pause at 400 rpm. $LiBH_4$ was recrystallized in $(C_2H_5)_2O$ and dried *in vacuo* at 90 °C. $PrCl_3$ and $LiBH_4$ were mixed in $C_6H_5CH_3$ and stirred for five days. The suspension was refluxed at 90 °C for 3 h. The $C_6H_5CH_3$ was then removed *in vacuo* at room temperature (RT) for 4 h. $S(CH_3)_2$ was added and the solution stirred for two days before removal of the $S(CH_3)_2$ *in vacuo* at 120 °C for 2 h.

Characterization and thermal decomposition studies

Decomposition experiments were conducted in an in-house manufactured Sieverts type apparatus.[31] Decomposition of S2 and S4 was executed using a temperature ramp of 5 °C min^{-1} from RT to 400 °C under 3 bar hydrogen pressure, followed by a

Table 1 Compositions, synthesis methods and solvents of the investigated samples. Compositions, lattice parameters and space groups of products were determined by Rietveld refinement with PXD data at RT. Estimated standard deviations are given in parentheses

Sample	Reactants	Method	Products	Amount (wt%)	Unit cell (Å)	Space group
S1	$ErCl_3$–3$LiBH_4$	BM + $S(CH_3)_2$ + heat treatment	α-$Er(BH_4)_3$	98.4(1)	a = 10.78517(7)	$Pa\bar{3}$
			β-$Er(BH_4)_3$	1.6(1)	a = 5.478(1)	$Pm\bar{3}m$
S2	$ErCl_3$–3$LiBH_4$	BM + $S(CH_3)_2$ + heat treatment	α-$Er(BH_4)_3$	87.8(1)	a = 10.76796(5)	$Pa\bar{3}$
			β-$Er(BH_4)_3$	12.2(1)	a = 5.4664(1)	$Pm\bar{3}m$
S3	$PrCl_3$–3$LiBH_4$	$(C_2H_5)_2O$	α-$Pr(BH_4)_3$	32.7(5)	a = 11.2465(1)	$Pa\bar{3}$
			$LiPr(BH_4)_3Cl$	35.8(5)	a = 11. 5468(3)	$I\bar{4}3m$
			$LiBH_4$	28.4(4)	a = 7.144(1)	$I\bar{4}3m$
					b = 4.421(1)	
					c = 6.779(2)	
			β-$Pr(BH_4)_3$	3.1(6)	a = 5.716(2)	$Pm\bar{3}m$
S4	$PrCl_3$–3$LiBH_4$	$C_6H_5CH_3$ + $S(CH_3)_2$	α-$Pr(BH_4)_3$		a = 11.2473(2)	$Pa\bar{3}$

21 h isothermal step. Hydrogen reabsorption for S2 was carried out at 340 °C, under 100 bar H_2, for 21 h. Furthermore, the decomposed S2 and S4 were physically mixed with 100 wt% LiCl and/or 50 wt% LiH with a mortar and pestle. The reabsorption was repeated at 400 °C under 100 bar H_2 followed by an 18 h isotherm.

Powder X-ray Diffraction (PXD) data were collected using a Rigaku SmartLab diffractometer. The data were collected in Debye–Scherrer transmission geometry using monochromatic $CuK_{\alpha 1}$ radiation, (λ = 1.54056 Å), a curved position-sensitive detector and scattering angle (2θ) 10–70°. The samples were contained within rotating glass capillaries with an inner diameter of 0.5 mm, sealed with silicone grease after filling.

In situ SR-PXD data were collected at the Swiss Norwegian Beam Line (SNBL), BM01A at the European Synchrotron Radiation Facility (ESRF), Grenoble, France. Sapphire capillaries were connected to an in-house manufactured remote controlled gas rig and high pressure manifold cell. The sapphire capillary was rotated by 10° to improve powder averaging. The sample-to-detector distance was 146 or 245.8 mm, respectively, and the wavelength was 0.69733 or 0.77787 Å, calibrated from a NIST LaB_6 standard. The *in situ* cycling experiments were conducted using a heating/cooling rate of 5 °C min^{-1} with a typical hydrogen pressure of ~100 bar for absorption and ~3 bar for desorption. Data were collected using a Pilatus 2M detector. The exposure time was set to 30 s giving a temperature resolution of 2.5 °C per pattern. Single crystal reflections from the sapphire tube were masked manually in Fit2D and Bubble.[32,33] The Rietveld refinements were performed using GSAS and Expgui software.[34,35] Three Gaussian and one Lorentzian parameter were modeled with a Thompson–Cox–Hastings pseudo-Voigt function.[36] The background was fitted with a shifted Chebyshev polynomial with up to 36 terms. Atomic positions for α- and β-$RE(BH_4)_3$ (RE = Er, Pr) and $LiPr(BH_4)_3Cl$ were taken from $Y(BH_4)_3$ (ref. 1 and 6) and $LiCe(BH_4)_3Cl$ (ref. 18), respectively, and not refined.

Simultaneous thermogravimetric and differential scanning calorimetry (TG-DSC) was conducted on S1–S4 using a Netzsch STA 449 F3 Jupiter analyzer. Samples were loaded in aluminum crucibles (~5–10 mg) and heated from RT to 400 °C at a heating rate of 5 °C min^{-1}. An argon flow of 20 ml min^{-1} was set as a protection gas flow with a purge gas rate of 50 ml min^{-1}.

S2 and S4 were measured by temperature programmed desorption (TPD-MS) in an in-house manufactured apparatus connected to a MKS Microvision-IP Rest Gas Analyser. The powders (~50 mg) were loaded in a steel sample holder and heated from RT to 400 °C with a heating rate of 5 °C min^{-1} under dynamic vacuum. S3 was measured by mass spectrometry (MS) using a Netzsch STA449C analyzer connected to a Hiden Analytical HPR-20 QMS. Samples (~5–10 mg) were loaded in aluminum-oxide crucibles and heated to 500 °C at a heating rate of 5 °C min^{-1}. An argon flow of 20 ml min^{-1} was set as a protection gas flow, while purge gas rate was 30 ml min^{-1}.

Results

Investigation of erbium borohydride

Fig. 1 shows Rietveld refinements at RT for the SR-PXD data of S1 and S2. Two phases are present in the samples which were identified as α-$Er(BH_4)_3$ and β-$Er(BH_4)_3$, respectively.[1,6] α-$Er(BH_4)_3$ crystallizes in the space group $Pa\bar{3}$, while β-$Er(BH_4)_3$ crystallizes in $Pm\bar{3}m$. Neither starting materials ($LiBH_4$, $ErCl_3$) nor by-products (LiCl) are observed. For S1, the phase fractions were refined to 98.4(1) wt% for α-$Er(BH_4)_3$ and 1.6(1) wt% for β-$Er(BH_4)_3$. For S2, the phase fractions were determined to 87.8(1) and 12.2(1) wt% for α- and β-$Er(BH_4)_3$, respectively.

The combined TPD-MS and TG-DSC data of S2 is shown in Fig. 2a. S2 releases 4.7 wt% of gas between RT and 400 °C. The slope of the TG measurement indicates a smooth decomposition event; starting at 184 °C with a moderate slope which gradually becomes steeper. The endothermic event observed by DSC has a peak maximum at 281 °C which correspond to the steepest slope of the TG curve. A possible decomposition pathway is:[37]

$$Er(BH_4)_3 \rightarrow 0.75ErB_4 + 0.25ErH_2 + 5.75H_2\ (5.4\ wt\%\ H_2) \quad (1)$$

The theoretical mass loss in eqn (1) is 5.4 wt% H_2 which is 14% more than the observed mass loss. The difference could be due

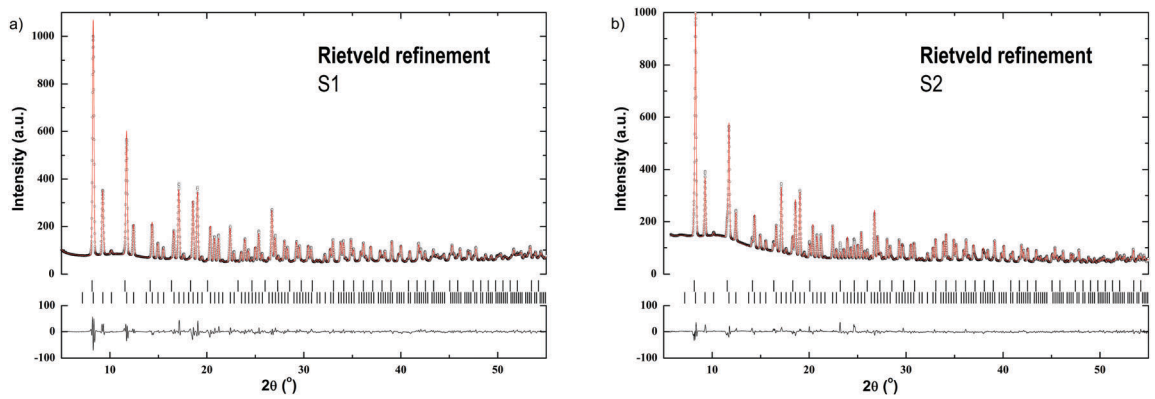

Fig. 1 (a) Rietveld refinement with the SR-PXD data of S1 at RT showing experimental (circles) and calculated (red line) patterns and a difference plot (below). Vertical ticks mark the Bragg peak positions for (from top): β-$Er(BH_4)_3$, α-$Er(BH_4)_3$. R_{wp} = 4.01%. λ = 0.77787 Å; (b) Rietveld refinement with the SR-PXD data of S2 at RT showing experimental (circles) and calculated (red line) patterns and a difference plot (below). Vertical ticks mark the Bragg peak positions for (from top): β-$Er(BH_4)_3$, α-$Er(BH_4)_3$. R_{wp} = 3.53%. λ = 0.77787 Å.

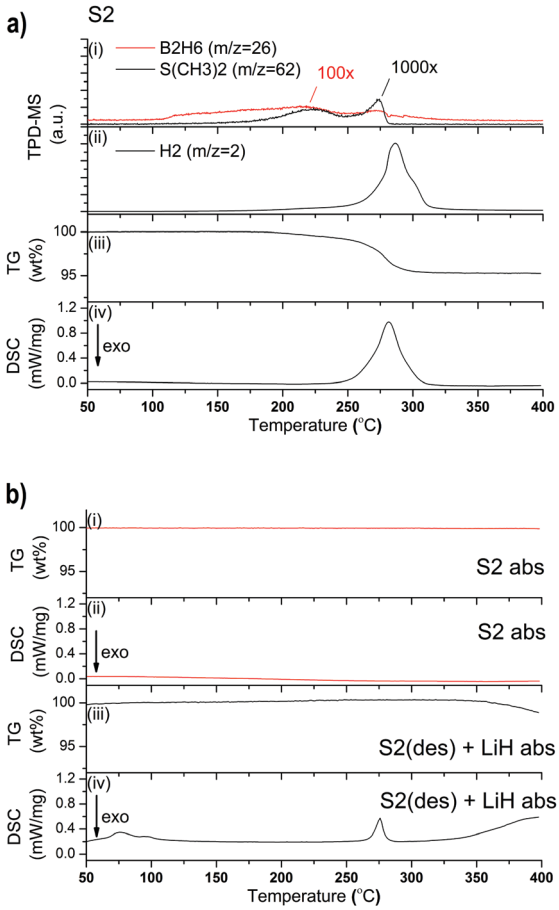

Fig. 2 (a) TPD-MS-TG-DSC analysis from RT to 400 °C of S2 showing release of $S(CH_3)_2$ and B_2H_6 (i), H_2 (ii), TG data (iii) and DSC signal (iv); (b) TG data (i) and DSC signal (ii) of S2 absorbed (red) and TG data (iii) and DSC signal (iv) of S2(des) + LiH absorbed (black) (temperature ramp of 5 °C min^{-1}).

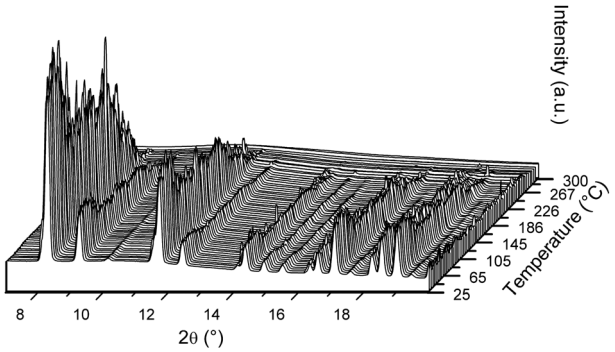

Fig. 3 *In situ* SR-PXD data from the desorption process of S2 between RT and 300 °C under 1 bar H_2 (temperature ramp of 5 °C min^{-1}). Rietveld refinements with phase composition for initial state (front) are given in Fig. 1b. See text for discussion. λ = 0.77787 Å.

to some decomposition during solvent removal step, higher H content in the erbium hydride phase or a different reaction pathway than the proposed one. In Fig. 2a(ii) the TPD-MS analysis shows H_2 as the majority gas desorbed. The temperature at which the peak is observed (286 °C) is in good agreement with that of the decomposition event from DSC data (281 °C). A shoulder is also seen to the right of the main decomposition event at 301 °C of which the exact process remains undetermined. Minor amounts of B_2H_6 and $S(CH_3)_2$ are also released with at least 2 orders of magnitude lower intensity than H_2 (Fig. 2a(i)).

For S2, one desorption–absorption-cycle was performed in the Sieverts-type apparatus. The desorption was performed at a heating rate of 5 °C min^{-1} from RT to 400 °C, followed by a 21 h isothermal step. A 3 bar H_2 pressure was employed during desorption which is reported to increase reversibility compared to samples desorbed in vacuum.[23,37,38] Absorption was performed at 340 °C under 100 bar H_2 for 21 h. However, the TG-DSC measurement of the absorbed sample shown in Fig. 2b (S2 abs) indicates that rehydrogenation has not occurred during this experiment.

Fig. 3 illustrates the *in situ* SR-PXD desorption data of pristine S2 from RT to 300 °C, under 1 bar H_2. This measurement confirms that all Bragg peaks of $Er(BH_4)_3$ have disappeared by 300 °C, which is consistent with the TG-DSC data, showing that decomposition is complete by ~300 °C. After cooling to RT, no crystalline reaction product is observed (not shown). At the end of the measurement, the background is slightly modulated, which may be indicative of nanocrystalline or amorphous phases. The Bragg peak intensities in the *in situ* SR-PXD measurement of S2 fluctuate significantly from exposure to exposure. The reason for which remains undetermined.

Investigation of praseodymium borohydride

S3 was synthesized in $(C_2H_5)_2O$, the LiCl by-product was removed by filtration and the solvent was then evaporated *in vacuo* (see Table 1). S4 was synthesized in $C_6H_5CH_3$ and extracted with $S(CH_3)_2$. The Rietveld refinement plots of S3 and S4 are shown in Fig. 4. The refinement of S3 reveals a mixture of α-$Pr(BH_4)_3$ crystallized in space group $Pa\bar{3}$[1] and β-$Pr(BH_4)_3$ in $Pm\bar{3}m$,[39] as well as $LiBH_4$ and $LiPr(BH_4)_3Cl$ in space groups *Pnma* and $I\bar{4}3m$, respectively.[5,18] No traces of the $PrCl_3$ starting material is observed in S3. The residual powder, after filtration, was also analyzed by PXD, indicating the presence of $PrCl_3$ and LiCl and thus suggesting that the reaction did not go to completion (Fig. A1, ESI†).

MS analysis of S3 reveals that H_2 release begins at 175 °C and continues through multiple desorption events until 375 °C (Fig. 5a(ii)). $(C_2H_5)_2O$ release is observed between 75 and 150 °C, while minor quantities of B_2H_6 are observed in a rather narrow range between 175 and 200 °C (Fig. 5a(i)). The TG data in Fig. 5a(iii) shows a release of 11.7 wt% and the DSC data reveals that it is a multistep process, with at least six major endothermic events. The first DSC peak can be assigned to the phase transition of orthorhombic-$LiBH_4$ (o-$LiBH_4$) to hexagonal-$LiBH_4$ (h-$LiBH_4$). The second peak at 176 °C can be attributed to the decomposition of $LiPr(BH_4)_3Cl$ as it coincides with mass loss observed by TG. The same decomposition process is observed at 191 °C during *in situ* SR-PXD, however, that reaction occurred under hydrogen pressure which shifts the reaction to higher temperature (Fig. 6a). A third, minor peak at 191 °C, which is also observed for S4 (Fig. 5b), could not be assigned to any known process, but is most likely correlated to a structural

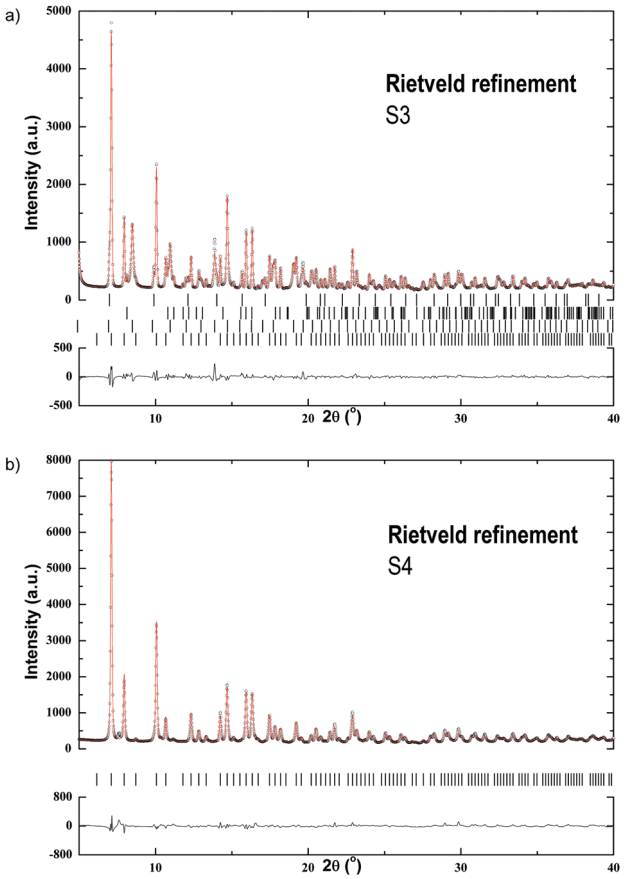

Fig. 4 (a) Rietveld refinement with the SR-PXD data of S3 at RT showing experimental (circles) and calculated (red line) patterns and a difference plot (below). Vertical ticks mark the Bragg peak positions for (from top): β-$Pr(BH_4)_3$, o-$LiBH_4$, $LiPr(BH_4)_3Cl$ and α-$Pr(BH_4)_3$. R_{wp} = 4.78%. λ = 0.69733 Å; (b) Rietveld refinement with the SR-PXD data of S4 at RT showing experimental (circles) and calculated (red line) patterns and a difference plot (below). Vertical ticks mark the Bragg peak positions for: α-$Pr(BH_4)_3$. R_{wp} = 6.25%. λ = 0.69733 Å.

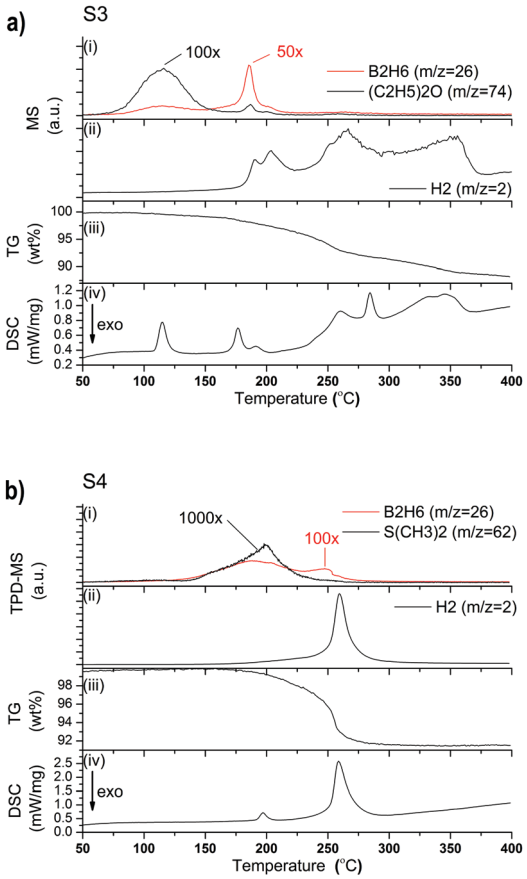

Fig. 5 (a) MS-TG-DSC analysis from RT to 400 °C of S3 showing release of $(C_2H_5)_2O$ and B_2H_6 (i), H_2 (ii), TG data (iii) and DSC signal (iv); (b) (TPD-MS)-TG-DSC analysis from RT to 400 °C of S4 showing release of $S(CH_3)_2$ and B_2H_6 (i), H_2 (ii), TG data (iii) and DSC signal (iv).

phase transition, as discussed for S4 below. The endothermic peak at 260 °C is probably the decomposition of the parent borohydride. Further peaks at 284 and 345 °C have not yet been assigned, but are probably related to the multistep decomposition of the borohydride species and unknown formation, as observed in the *in situ* SR-PXD (Fig. 6a), which coincides again with the mass loss of 8.6 wt% between 200 and 360 °C.

The *in situ* decomposition of S3 studied by SR-PXD is shown in Fig. 6a and supports the multistep decomposition pathway suggested from the DSC data. The sample was heated from RT to 500 °C at a ramp of 5 °C min^{-1}, followed by cooling to RT. At 103 °C, the phase transition of o-$LiBH_4$ to h-$LiBH_4$ is observed. The Bragg peaks of $LiPr(BH_4)_3Cl$ and α-$Pr(BH_4)_3$ disappear at 191 °C and 230 °C, respectively. A third phase, possibly a alternative polymorph of $Pr(BH_4)_3$, disappears at 282 °C. New Bragg peaks appear at 214 °C and vanish at 318 °C, which could originate from PrH_3. From 346 °C, a second new phase appears and is the only crystalline phase in the pattern until 413 °C, when it starts to decrease to a minimum at 506 °C. PrB_6 is observed from 399 °C, becomes the major phase until 507 °C and remains after cooling to RT.

The SR-PXD pattern for S4 at RT is shown in Fig. 4b. The diffraction pattern is distinctively different to that of S3, which is due to removal of $S(CH_3)_2$, LiCl and $LiBH_4$. The refined parameters are given in Table 1. Fig. 5b(i–iv) shows TPD-MS and TG-DSC data of S4. A phase transition is observed in the DSC data at 192 °C. S4 loses ~8.3 wt% when heated from RT to 400 °C.

$$Pr(BH_4)_3 \rightarrow 0.5PrB_6 + 0.5PrH_2 + 5.5H_2\ (5.7\ wt\%\ H_2) \quad (2)$$

Most of the weight loss can be assigned to the decomposition of the RE borohydride (eqn (2)). The TPD-MS analysis (Fig. 5b(i and ii)) shows that the majority of the desorbed gas is H_2, which is in good agreement with the decomposition event from DSC data. Minor amounts of B_2H_6 and $S(CH_3)_2$ were released, and are possibly responsible for the difference between the theoretical and measured H_2 capacity. This leads to the assumption that not all solvent was removed during synthesis.

The *in situ* SR-PXD decomposition of S4 between RT and 500 °C is shown in Fig. 6b. During heating from RT to 204 °C, the pattern is dominated by α-$Pr(BH_4)_3$ crystallized in space group $Pa\bar{3}^1$ with a = 11.2473(2) Å at RT. At 204 °C, a structural phase transition occurs, which is consistent with our DSC data. Bragg peaks from the high temperature $Pr(BH_4)_3$ phase increase in intensity until 217 °C and vanish at 275 °C, after which no more

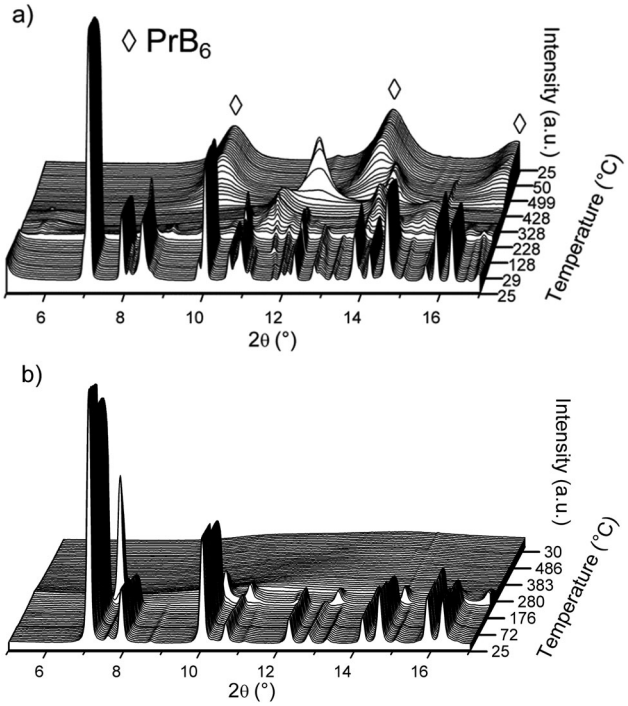

Fig. 6 *In situ* SR-PXD of decomposition reaction of S3 (a) and S4 (b) heated from RT to 500 °C (temperature ramp of 5 °C min^{-1}) and cooling to RT. Rietveld refinements with phase composition for initial state (front) are given in Fig. 4. See text for discussion. λ = 0.69733 Å.

crystalline products are observed. After reaching 500 °C, the sample is cooled to RT without appearance of any crystalline compounds.

The influence of LiH

Both the *ex* and *in situ* SR-PXD measurements show that hydrogen is not reversibly stored in S2. This is in disagreement with Gennari who reported that the $Er(BH_4)_3$, synthesized by ball milling, had a reversibility of 20% at 400 °C, under 60 bar H_2.[24] However, this may be attributed to the presence of Li-ions in the sample, with a formation of $LiBH_4$ instead of regenerating $Er(BH_4)_3$. In our *in situ* SR-PXD absorption study, 100 bar H_2 was applied to the decomposed sample at the same temperature and this time crystalline metal borohydride products were not observed. This is in agreement with the absorption experiment carried out in the Sieverts-type apparatus at 340 °C, under 100 bar H_2. Furthermore, the lack of reversibility was confirmed by our TG-DSC measurements (Fig. 2b). Overall, this suggests an altered decomposition pathway in our halide free $Er(BH_4)_3$. In the absence of LiCl, the formation of amorphous and/or nanocrystalline phases occurs during decomposition without formation of crystalline phases upon rehydrogenation.

In order to corroborate this assumption, the decomposition product of S2 was physically mixed in a 1 : 1 mass ratio with LiCl. The hydrogenation experiment was carried out *in* and *ex situ* without the resultant appearance of any crystalline rehydrogenation products (*in situ* SR-PXD in Fig. A2; TG-DSC in Fig. A3, ESI†). The experiment was repeated with addition of 50 wt% of LiH to desorbed S2 instead of LiCl, as LiH is less stable than LiCl. The hydrogenation process was followed *in situ* at 400 °C, under 100 bar H_2. The products of this reaction are ErH_3 and $LiBH_4$, as shown in Fig. 7. ErH_3 is formed at 400 °C (* in Fig. 7). During cooling to RT the h-$LiBH_4$ appears at 268 °C. The transition to o-$LiBH_4$ is also detected, which is in agreement with our DSC data, shown in Fig. 2b(iv), in which the presence of $LiBH_4$ is suggested by the phase transition of o- to h-$LiBH_4$ at 97 °C. The process behind the endothermic event at 74 °C is undetermined. In our sample, melting is observed at 272 °C, which is strongly indicative of the presence of $LiBH_4$. The TG data in Fig. 2b shows that 1 wt% H_2 is released during heating to 400 °C, probably linked to the decomposition of $LiBH_4$.

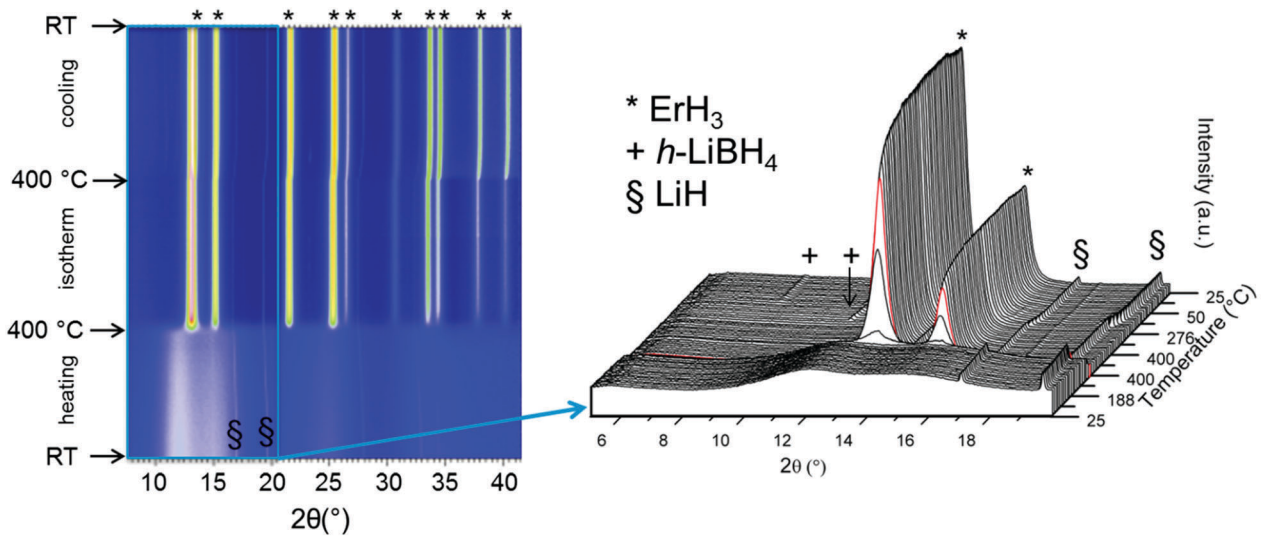

Fig. 7 *In situ* SR-PXD data of a powder mixture containing desorbed S2 + 50 wt% LiH. The composite was heated from RT to 400 °C with a 1 h isothermal stage and cooling to RT in $p(H_2)$ = 100 bar (temperature ramp of 5 °C min^{-1}). Inset showing magnification of the 2θ range 5 to 20° to enhance the visibility of the appearance of Bragg peaks for h-$LiBH_4$ (+). Red curve in magnification marks the temperature of 400 °C. λ = 0.69733 Å.

For the *ex situ* desorbed S4, the PXD pattern (not shown) did not show any crystalline phases. Thus, we assume that the reaction mechanism is the same as for S2. Therefore, 50 wt% of LiH was mixed with desorbed S4 (Fig. A4, ESI†) and rehydrogenation was carried out *ex situ* using the same conditions. PXD data (Fig. A5, ESI†) indicates the product PrH_2 while TG-DSC data (Fig. A6, ESI†) indicates the formation of $LiBH_4$. A weight loss of 1.7 wt% H_2 is observed by TG. The observation of $LiBH_4$ can often be very difficult in diffraction experiments since the scattering of $LiBH_4$ is weak.

Discussion

For sample S2, two $Er(BH_4)_3$ polymorphs are detected at RT by SR-PXD. Earlier reports have shown a slight deviation in products. Olsen *et al.* observed only the β-$Er(BH_4)_3$ polymorph after 5 h of mechanochemical synthesis from $ErCl_3$ and $3LiBH_4$.[13] After annealing at 100 °C for 50 h, the α-$Er(BH_4)_3$ crystallized and replaced the metastable β-$Er(BH_4)_3$ polymorph.[13] In contrast, Gennari reported that only the α-$Er(BH_4)_3$ polymorph was formed by mechanochemical synthesis.[24] The differences in reports may be a result of the different pause time used during mechanochemical synthesis. Gennari describes the synthesis with 10 min milling followed by 10 min pause,[24] opposed to Olsen *et al.* who milled for 5 h without breaks.[13] Gennari also reported a reversible phase transition from α-$Er(BH_4)_3$ to β-$Er(BH_4)_3$ at 220 °C, which was neither determined in our DSC measurements, nor during our *in situ* SR-PXD analysis. Olsen *et al.* only observed a decrease of the parent borohydride Bragg peaks, and an increasing background during *in situ* SR-PXD while heating from 170–210 °C.[13] However, the polymorphic transition is not observed in our study. To summarize, it seems that the reaction conditions have a major influence on the formation of the different $Er(BH_4)_3$ polymorphs. S1 primarily consists of α-$Er(BH_4)$ (98.4(1) wt%), along with β-$Er(BH_4)_3$ (1.6(1) wt%) (Fig. 1a), while in S2, it is approximately a 9 : 1 ratio of α-$Er(BH_4)_3$ to β-$Er(BH_4)_3$ (Fig. 1b). Thus, milder reaction conditions appear to favor the formation of α-$Er(BH_4)_3$.

The modulated background and the poor crystallinity of S2 during *in situ* SR-PXD can be compared with a recent *in situ* decomposition study, where solvent extracted $Gd(BH_4)_3$ was investigated.[16] The intensity of Bragg peaks belonging to $Gd(BH_4)_3$ decreases between 180 and 270 °C, where after poor crystallinity and a modulated background is observed between 270 and 400 °C. This temperature region is the same as where pristine S2 becomes amorphous and a modulated background is observed.

The theoretical hydrogen capacity for the decomposition reaction of S2, according to eqn (1) is 5.4 wt%. Thus, the 4.7 wt% measured is 13% lower than expected. This deviation could be attributed to incomplete decomposition and the formation of a combination of different ErH_x phases and/or the combination of nanocrystalline $ErH_{2+\delta}$ and ErH_3 as reported recently.[37,40,41] The peak temperature of decomposition in our DSC measurement is 10–20 °C higher compared to earlier reports.[24] However, the Ar flow rate was about 50% lower compared to former reports, while heating rates were consistent at 5 °C min^{-1}.[24] Olsen *et al.* used the same conditions for Ar flow, and heating rates, compared to the present experiments, but the decomposition temperature of $Er(BH_4)_3$, in the presence of six molar equivalents of $LiBH_4$, was 240 °C,[13,37] and thus lower compared to the decomposition temperature of S2 at 281 °C. As reported recently for $Y(BH_4)_3 + LiBH_4$, this decrease is probably an effect of the co-melt/decomposition of $Er(BH_4)_3$ and $LiBH_4$.[19,26,42] A similar result was found when pure $RE(BH_4)_2$ with RE = Eu, Sm[14] were compared to the impure compounds containing residual LiCl in the powder.[13,14] It was determined that the latter had a decreased decomposition temperature, probably caused by residual $LiBH_4$.[14] LiCl or $LiBH_4$ were not present in S2, which causes the higher decomposition temperature in our study.

The appearance of $LiBH_4$ during rehydrogenation with addition of 50 wt% LiH to both S2 and S4 was not simply a recrystallization effect. Our rehydrogenation of S2, without additional LiH, showed no endothermic peaks in the DSC data. Thus, it is strongly suggested, that there was no $LiBH_4$ in the sample. The reaction conditions are much milder compared to reported values of 155 bar H_2 and 600 °C for rehydrogenation of pure $LiBH_4$.[43] A control experiment with the addition of LiCl was not successful, which again suggests that the influence of LiH on rehydrogenation goes beyond being a source of Li-ions. In analogy, the formation of $LiBH_4$ from hydrogenation of reactive hydride composites with LiH, such as LiH + MgB_2, are already known from literature, again under much harsher conditions or usage of catalysts.[44,45]

The effect of LiH is not fully understood, but one explanation as to why this effect has not been discovered earlier in metal borohydrides could be that LiH is a decomposition product of $LiBH_4$, which is a likely impurity phase in all metal borohydrides synthesized by mechanochemical synthesis. Unreacted $LiBH_4$ thus acts as a source for LiH during the thermal decomposition of such metal borohydrides. This can be very difficult to observe in diffraction experiments since the scattering of LiH is very weak and the Bragg peaks are often overlapped by other Bragg peaks, thus making LiH difficult to identify.

The first direct synthesis of $Pr(BH_4)_3$ has been shown in S3 by the solvation method. By itself, $(C_2H_5)_2O$ facilitates the production of α-$Pr(BH_4)_3$, $LiPr(BH_4)_3Cl$ and minor amounts of β-$Pr(BH_4)_3$. α-$Pr(BH_4)_3$ crystallizes in space group $Pa\bar{3}$, which is analogous to α-$Y(BH_4)_3$.[6] S4 on the other hand shows that extraction with $S(CH_3)_2$ removes LiCl and forms α-$Pr(BH_4)_3$ (see Fig. 4b).

The attempt to synthesize $Pr(BH_4)_3$ halide free for the first time was partly successful. Unwanted LiCl impurities could not be removed entirely, which led to formation of $LiPr(BH_4)_3Cl$ in S3. The decomposition pathways of S3 and S4 are completely different, which is assumed to be an effect of the remaining LiCl. It seems to play a crucial role in the decomposition pathway of S3, as decomposition is rather complex with at least six major endothermic events. Decomposition of S4 without LiCl is rather simple. This opposed behavior suggests that the LiCl has a role beyond being an inert "dead mass" compound.

Conclusions

Two new halide free RE borohydrides, $Er(BH_4)_3$ and $Pr(BH_4)_3$, have been synthesized. $Er(BH_4)_3$, synthesized *via* mechanochemical synthesis followed by solvent extraction shows a deviation in behavior compared to previous mechanochemical synthesis containing the reaction product LiCl.[24] In the absence of any LiCl, the reaction pathway during *in situ* SR-PXD decomposition of $Er(BH_4)_3$ indicates that the reaction products are completely amorphous. Rehydrogenation of the decomposition products at 400 °C under 100 bar H_2 was unsuccessful.

To prove the assumption that the absence of LiCl is responsible for the amorphous decomposition product(s) of S2 and negligible rehydrogenation, the desorbed sample was mixed with LiCl, without any effect upon rehydrogenation. The physical mixture of the desorbed $Er(BH_4)_3$ with 50 wt% of LiH was also investigated upon rehydrogenation, as LiH is less stable than LiCl. At 400 °C, under 100 bar H_2, the crystalline reaction products, ErH_3 and $LiBH_4$, appeared during cooling. The same reaction mechanism occurred for the desorbed $Pr(BH_4)_3$ + 50 wt% LiH sample. PrH_2 and $LiBH_4$ were formed upon rehydrogenation at the same conditions. Thus, the presence of LiH improves the crystallinity and rehydrogenation properties.

An attempt to increase the total hydrogen storage capacity by the investigation of a $4LiBH_4 + ErH_3$ composite was unsuccessful. PXD analyses (Fig. A7, ESI†) reveals, that the composite cannot be cycled between $4LiBH_4 + ErH_3$ and $ErB_4 + 4LiH + 7.5H_2$ at the conditions described above. This observation reveals that erbium hydride needs to be formed *in situ* to have a destabilization effect on $LiBH_4$. This is also in agreement with Gennari *et al.* who investigated a $4LiBH_4 + YH_3$ composite and also showed the superior destabilization of $LiBH_4$ by *in situ* formed YH_3.[23] Anyhow, ErH_3 synthesized directly from the elements is not able to destabilize $LiBH_4$ (for further information see Fig. A7 and A8 in the ESI†).

The $Pr(BH_4)_3$ synthesized in $(C_2H_5)_2O$ alone, shows that $LiPr(BH_4)_3Cl$ is also formed in tandem with $Pr(BH_4)_3$, while recrystallization from $S(CH_3)_2$ and further heat treatment produced almost pure α-$Pr(BH_4)_3$. This material undergoes a phase transition during heating at 192 °C, although the nature of this phase transition will be studied in a follow up investigation.

In summary, we have synthesized pure $RE(BH_4)_3$, making it possible to investigate properties on the pure RE borohydrides. Additionally, the full gravimetric hydrogen content of these materials is now available. The supporting role of LiH was found to be essential for reversibility towards the formation of RE hydrides and $LiBH_4$.

Acknowledgements

The research leading to these results has received funding from the People Program (Marie Curie Actions) of the European Union's Seventh Framework Program FP7/2007-2013/under REA grant agreement no. 607040 (Marie Curie ITN ECOSTORE) and the Innovation Fund Denmark (project HyFill-Fast) and is thankfully acknowledged. We also acknowledge Prof. Radovan Černý for his scientific input and the Research Council of Norway for financial assistance. The authors acknowledge the skillful assistance from the staff of the Swiss-Norwegian Beamline, at the European Synchrotron Radiation Facility, Grenoble, France.

Notes and references

1 T. Sato, K. Miwa, Y. Nakamori, K. Ohoyama, H.-W. Li, T. Noritake, M. Aoki, S.-i. Towata and S.-i. Orimo, *Phys. Rev. B: Condens. Matter Mater. Phys.*, 2008, **77**, 104114.
2 J. E. Olsen, C. Frommen, M. H. Sørby and B. C. Hauback, *RSC Adv.*, 2013, **3**, 10764–10774.
3 T. Jaroń and W. Grochala, *Dalton Trans.*, 2010, **39**, 160–166.
4 C. Frommen, N. Aliouane, S. Deledda, J. E. Fonneløp, H. Grove, K. Lieutenant, I. Llamas-Jansa, S. Sartori, M. H. Sørby and B. C. Hauback, *J. Alloys Compd.*, 2010, **496**, 710–716.
5 C. Frommen, M. H. Sørby, P. Ravindran, P. Vajeeston, H. Fjellvåg and B. C. Hauback, *J. Phys. Chem. C*, 2011, **115**, 23591–23602.
6 D. B. Ravnsbæk, Y. Filinchuk, R. Černý, M. B. Ley, D. r. Haase, H. J. Jakobsen, J. r. Skibsted and T. R. Jensen, *Inorg. Chem.*, 2010, **49**, 3801–3809.
7 M. B. Ley, L. H. Jepsen, Y.-S. Lee, Y. W. Cho, J. M. B. von Colbe, M. Dornheim, M. Rokni, J. O. Jensen, M. Sloth and Y. Filinchuk, *Mater. Today*, 2014, **17**, 122–128.
8 Y. Yan, H.-W. Li, T. Sato, N. Umeda, K. Miwa, S.-i. Towata and S.-i. Orimo, *Int. J. Hydrogen Energy*, 2009, **34**, 5732–5736.
9 T. Jaron, W. Kozminski and W. Grochala, *Phys. Chem. Chem. Phys.*, 2011, **13**, 8847–8851.
10 F. C. Gennari and M. R. Esquivel, *J. Alloys Compd.*, 2009, **485**, L47–L51.
11 H.-W. Li, Y. Yan, S.-i. Orimo, A. Züttel and C. M. Jensen, *Energies*, 2011, **4**, 185–214.
12 B. J. Zhang, B. H. Liu and Z. P. Li, *J. Alloys Compd.*, 2011, **509**, 751–757.
13 J. E. Olsen, C. Frommen, T. R. Jensen, M. D. Riktor, M. H. Sørby and B. C. Hauback, *RSC Adv.*, 2014, **4**, 1570–1582.
14 T. D. Humphries, M. B. Ley, C. Frommen, K. T. Munroe, T. R. Jensen and B. C. Hauback, *J. Mater. Chem. A*, 2015, **3**, 691–698.
15 R. Černý, D. B. Ravnsbæk, G. Severa, Y. Filinchuk, V. D'Anna, H. Hagemann, D. Haase, J. Skibsted, C. M. Jensen and T. R. Jensen, *J. Phys. Chem. C*, 2010, **114**, 19540–19549.
16 M. B. Ley, S. Boulineau, R. Janot, Y. Filinchuk and T. R. Jensen, *J. Phys. Chem. C*, 2012, **116**, 21267–21276.
17 A. V. Skripov, A. V. Soloninin, M. B. Ley, T. R. Jensen and Y. Filinchuk, *J. Phys. Chem. C*, 2013, **117**, 14965–14972.
18 M. B. Ley, D. B. Ravnsbæk, Y. Filinchuk, Y.-S. Lee, R. l. Janot, Y. W. Cho, J. Skibsted and T. R. Jensen, *Chem. Mater.*, 2012, **24**, 1654–1663.
19 E. Roedern, Y.-S. Lee, M. B. Ley, K. Park, Y. W. Cho, J. Skibsted and T. R. Jensen, *J. Mater. Chem. A*, 2016, **4**, 8793–8802.
20 S. Marks, J. G. Heck, M. H. Habicht, P. Oña-Burgos, C. Feldmann and P. W. Roesky, *J. Am. Chem. Soc.*, 2012, **134**, 16983–16986.

21 P. Schouwink, M. B. Ley, A. Tissot, H. Hagemann, T. R. Jensen, L. Smrčok and R. Černý, *Nat. Commun.*, 2014, **5**, 5706.
22 P. Schouwink, E. Didelot, Y.-S. Lee, T. Mazet and R. Černý, *J. Alloys Compd.*, 2016, **664**, 378–384.
23 F. Gennari, L. F. Albanesi, J. Puszkiel and P. A. Larochette, *Int. J. Hydrogen Energy*, 2011, **36**, 563–570.
24 F. C. Gennari, *J. Alloys Compd.*, 2013, **581**, 192–195.
25 B. James and M. Wallbridge, *Prog. Inorg. Chem.*, 1970, **11**, 99–231.
26 M. B. Ley, M. Paskevicius, P. Schouwink, B. Richter, D. A. Sheppard, C. E. Buckley and T. R. Jensen, *Dalton Trans.*, 2014, **43**, 13333–13342.
27 M. Visseaux and F. Bonnet, *Coord. Chem. Rev.*, 2011, **255**, 374–420.
28 H. Hagemann, M. Longhini, J. W. Kaminski, T. A. Wesolowski, R. Černý, N. Penin, M. H. Sørby, B. C. Hauback, G. Severa and C. M. Jensen, *J. Phys. Chem. A*, 2008, **112**, 7551–7555.
29 R. Černý, G. Severa, D. B. Ravnsbæk, Y. Filinchuk, V. D'Anna, H. Hagemann, D. Haase, C. M. Jensen and T. R. Jensen, *J. Phys. Chem. C*, 2009, **114**, 1357–1364.
30 L. Huang, O. Elkedim and X. Li, *J. Alloys Compd.*, 2012, **536**, S546–S549.
31 H. Brinks, A. Fossdal, R. Bowman and B. C. Hauback, *J. Alloys Compd.*, 2006, **417**, 92–95.
32 A. Hammersley, *Rep., ESRF97HA02T*, 1997.
33 V. Dyadkin, P. Pattison, V. Dmitriev and D. Chernyshov, *J. Synchrotron Radiat.*, 2016, **23**, 825–829.
34 A. Larson and R. Von Dreele, *General Structure Analysis System (GSAS); Report LAUR 86-748*; Los Alamos National Laboratory, Los Alamos, NM, 2000.
35 B. H. Toby, *J. Appl. Crystallogr.*, 2001, **34**, 210–213.
36 P. Thompson, D. Cox and J. Hastings, *J. Appl. Crystallogr.*, 1987, **20**, 79–83.
37 C. Frommen, M. Heere, M. D. Riktor, M. H. Sørby and B. C. Hauback, *J. Alloys Compd.*, 2015, **645**(suppl 1), S155–S159.
38 J.-H. Shim, J.-H. Lim, S.-u. Rather, Y.-S. Lee, D. Reed, Y. Kim, D. Book and Y. W. Cho, *J. Phys. Chem. Lett.*, 2010, **1**, 59–63.
39 Y.-S. Lee, J.-H. Shim and Y. W. Cho, *J. Phys. Chem. C*, 2010, **114**, 12833–12837.
40 F. C. Gennari, *Int. J. Hydrogen Energy*, 2011, **36**, 15231–15238.
41 M. Heere, S. H. Payandeh GharibDoust, C. Frommen, M. H. Sørby, T. R. Jensen and B. C. Hauback, 2016, to be submitted.
42 K. Park, H.-S. Lee, A. Remhof, Y.-S. Lee, Y. Yan, M.-Y. Kim, S. J. Kim, A. Züttel and Y. W. Cho, *Int. J. Hydrogen Energy*, 2013, **38**, 9263–9270.
43 P. Mauron, F. Buchter, O. Friedrichs, A. Remhof, M. Bielmann, C. N. Zwicky and A. Züttel, *J. Phys. Chem. B*, 2008, **112**, 906–910.
44 G. Barkhordarian, T. Klassen, M. Dornheim and R. Bormann, *J. Alloys Compd.*, 2007, **440**, L18–L21.
45 J. J. Vajo, S. L. Skeith and F. Mertens, *J. Phys. Chem. B*, 2005, **109**, 3719–3722.